Received: 14 June 2019 | Revised: 23 August 2019 | Accepted: 6 September 2019

DOI: 10.1002/nag.3007

RESEARCH ARTICLE

WILEY

Modeling cyclic shearing of sands in the semifluidized state

Andres R. Barrero[1] | **Mahdi Taiebat**[1] | **Yannis F. Dafalias**[2,3]

[1]Department of Civil Engineering, University of British Columbia, Vancouver, British Columbia, Canada

[2]Department of Civil and Environmental Engineering, University of California, Davis, California, U.S.A.

[3]Department of Mechanics, Faculty of Applied Mathematical and Physical Sciences, National Technical University of Athens, Athens, Greece

Correspondence
Mahdi Taiebat, 6250 Applied Science Lane, Vancouver, British Columbia V6T 1Z4, Canada.
Email: mtaiebat@civil.ubc.ca

Funding information
Division of Civil, Mechanical and Manufacturing Innovation, Grant/Award Number: 1162096; FP7 Ideas: European Research Council, Grant/Award Number: 290963; General Secretariat for Research and Technology of Greece; Natural Sciences and Engineering Research Council of Canada

Summary

Liquefaction is associated with the loss of mean effective stress and increase of the pore water pressure in saturated granular materials due to their contractive tendency under cyclic shear loading. The loss of mean effective stress is linked to loss of grain contacts, bringing the granular material to a "semifluidized state" and leading to development and accumulation of large cyclic shear strains. Constitutive modeling of the cyclic stress-strain response in earthquake-induced liquefaction and post-liquefaction is complex and yet very important for stress-deformation and performance-based analysis of sand deposits. A new state internal variable named strain liquefaction factor is introduced that evolves at low mean effective stresses, and its constitutive role is to reduce the plastic shear stiffness and dilatancy while maintaining the same plastic volumetric strain rate in the semifluidized state. This new constitutive ingredient is added to an existing critical state compatible, bounding surface plasticity reference model, that is well established for constitutive modeling of cyclic response of sands in the pre-liquefaction state. The roles of the key components of the proposed formulation are examined in a series of sensitivity analyses. Their combined effects in improving the performance of the reference model are examined by simulating undrained cyclic simple shear tests on Ottawa sand, with focus on reproducing the increasing shear strain amplitude as well as its saturation in the post-liquefaction response.

KEYWORDS

constitutive modeling, cyclic, liquefaction, sand, semifluidized, shear strain accumulation

1 | INTRODUCTION

Past and recent earthquakes have consistently shown the damaging effects of soil liquefaction on civil structures. Understanding the fundamental mechanism behind soil liquefaction has been one of the major challenges in the geotechnical engineering community. The tendency of dry loose granular material to densify in either monotonic or cyclic shearing is well known. When saturated, rapid shearing leads to a nearly undrained condition and the contractive tendency of the material causes pore water pressure to increase and effective stress to decrease. Liquefaction phenomena that result from this process can be divided into groups of flow liquefaction and cyclic mobility.[1]

Flow liquefaction often occurs in very loose granular media subjected to monotonic loading and is characterized by the sudden loss of strength. In this phenomenon, soil enters a state of instability, accompanied by a sudden increase in pore water pressure and shear strain. On the other hand, cyclic mobility can occur in medium to dense granular media and is characterized by consecutive cycles of loss and gain of effective stress in cyclic loading, resulting in temporary loss of stiffness, hence generation and accumulation of shear strains in each load cycle that essentially happens at the

state of very small effective stress. This state, referred to as "semi-suspended,"[2] will be addressed as "semifluidized" (Sf) henceforth in this paper.

The event where the effective stress vanishes for the first time is termed "initial liquefaction,"[3] which separates the whole liquefaction process into "pre-liquefaction" stage and "post-liquefaction" stage. Large post-liquefaction shear deformation is one of the major hazards encountered as a result of cyclic mobility and it has been recursively studied after observation in the Niigata earthquake in 1964. Laboratory studies on undrained cyclic shearing of sand show excessive accumulation of shear strains in the post-liquefaction response.[4,5] The main goal of this paper is modeling the shear strains that occur in the Sf state during the post-liquefaction cyclic loading in sands.

Several constitutive models have been developed over the years to simulate the stress-strain response of saturated sand under cyclic loading. These include, but are not limited to, the generalized plasticity models,[6,7] hypoplasticity models,[8,9] nested surface models,[10] and bounding surface models.[11-13] In the generalized plasticity model of Pastor et al,[7] the cyclic mobility is modeled by superseding the memory of the preceding cycles through the ratio of the maximum mobilized stress. This has resulted in the model response to be softer than observed from the experiments. In the hypoplastic model of Niemunis and Herle,[9] the concept of intergranular strain is used to reduce the soil stiffness upon unloading-reloading scenarios for capturing the cyclic degradation. The bounding surface plasticity model of Dafalias and Manzari[11] simulates the cyclic mobility by incorporating a fabric-dilatancy tensor, enhancing the contractive behavior upon unloading that follows a dilation state, thereby dragging the stress path to low effective stresses in undrained cyclic loading. Despite their elegant mathematical formulations and their success in a number of different aspects of response in the pre-liquefaction stage, the cyclic stress-strain loops in all of them tend to freeze very rapidly after the first liquefaction cycle, contrary to what is seen from the experiments.

To model the level of increasing shear strains in cyclic loading, various constitutive schemes have been proposed. In the nested surface model of Elgamal et al,[10] when the stress-ratio crosses the phase transformation line at low mean effective stresses (eg, less than 10 kPa)—referred to as the "neutral phase"—shear strain develops in the form of a perfectly plastic response, until a boundary defined in deviatoric strain space is reached. Other models, eg, Boulanger and Ziotopoulou,[13] have used a stiffness degradation as a function of cumulative shear strains to achieve the continual cyclic degradation observed in the experiments. Extending the original model by Zhang and Wang[4] in order to incorporate critical state compliance following various examples,[11,14,15] Wang et al[16] used various novel concepts such as splitting the dilatancy into reversible (also split in two parts) and irreversible components and introducing the concept of volumetric strain threshold below which the soil is considered liquefied. The model is quite capable of simulating several data including that of increasing shear strain amplitude successfully, but the formulation stays in the side of one that is rather complicated. These approaches have made practical contributions to the modeling of accumulation of shear strain in cyclic mobility; however, they share a shortcoming common to several similar models. They use either cumulative shear strain or cumulative irreversible volumetric strain as part of their formulation that stays as permanent fixtures in the model because there is no constitutive mechanism to eliminate their influence when it must. For example, if one changes from undrained cyclic to drained monotonic, the existing cumulative shear strain will affect the drained response unduly; furthermore, when cyclic loading resumes after drainage of a previous undrained cyclic event, these quantities that developed during the previous cyclic loading will affect the new one as if it were a continuation of the former, not a realistic consideration. One may try to delete (forget) the existing cumulative shear or irreversible volumetric strain upon initiating drained monotonic loading, but then again, what about if the drained monotonic loading is very small in duration and cyclic shearing resumes right after; will these preexisting cumulative strains begin to accumulate from zero or not? If they do, an unjustified response discontinuity will occur since a bit before and a bit after the very small drained monotonic loading, the cumulative strains will be nonzero and zero, respectively. On the other hand, if the shear strain, for example, is not forgotten when resuming drained monotonic loading, it will adversely affect the response because its role is related to undrained cyclic degradation that does not necessarily persist when drained monotonic loading is resumed. In essence, the problem is that the cumulative shear or irreversible volumetric strain during undrained cyclic loading continues to accumulate and affect the response in a subsequent drained monotonic or even cyclic loading unduly unless a mechanism for properly readjusting its effect is devised.

In this paper, the modeling of sand cyclic stress-strain response under constant volume conditions is explored by developing a novel constitutive tool aimed at degrading the stiffness and dilatancy when the material enters a semifluidized (Sf) state. Such state is reached when the mean effective stress p acquires values within the so-called Sf range defined by a relatively very small threshold p_{th}, ie, when $0 < p < p_{th}$. This stiffness and dilatancy degradation is removed without discontinuity when p abandons the Sf range. It should be noted that the constant volume condition can (but does not

need to) correspond to the undrained behavior. To this end, the paper first evaluates the undrained cyclic simple shear response from the laboratory test results of Parra[17] to obtain a detailed description of the Sf range. On that basis, a new state internal variable named strain liquefaction factor is introduced whose constitutive role is to induce the aforementioned degradation, and is formulated such that it evolves only at in the Sf state under constant volume conditions, while it resumes progressively its initial value upon subsequent loading associated with volume change and starts anew its role when a new constant volume cyclic loading is imposed. The proposed formulation is then incorporated into an existing stress-ratio-controlled, critical state-compatible, bounding surface plasticity model by Dafalias and Manzari,[11] which is well established for constitutive modeling of cyclic response of sands in the pre-liquefaction stage, to simulate large but bounded shear strains in the post-liquefaction stage of undrained cyclic simple shearing. The role of each one of the new model parameters is explained through a series of sensitivity analyses. Finally, the improved performance of the new model with the calibrated additional parameters is illustrated by simulating the pre- and the post-liquefaction response of cyclic simple shear tests on Ottawa sand and a cyclic torsional shear test or Toyoura sand. For definiteness, the new model will be referred to as SANISAND-Sf because it belongs to the SANISAND family of models and incorporates the new constitutive notion of Sf state.

2 | OBSERVATIONS FROM CYCLIC SIMPLE SHEAR TESTS

Much research has been carried out to investigate the cyclic shearing response of sands using laboratory experiments and numerical methods. In this section, special attention is given to evidence from a recent comprehensive database of experimental cyclic simple shear testing results on Ottawa F-65 sand and findings from a number of recent discrete element method (DEM) studies on assemblies of idealized grains.

Parra[17] reported a comprehensive database of undrained cyclic simple shear test on Ottawa F-65 sand involving the cyclic mobility, where details of the pre- and post-liquefaction responses can be explored. Figure 1A,B shows the stress path and stress-strain loops in one of these tests at D_r=77%. The loading process can be divided into stages of pre-liquefaction, shown in grey, and post-liquefaction, shown in black. In the pre-liquefaction stage, the mean effective stress in each cycle progressively diminishes as the cyclic loading continues. The third cycle of loading shown with a dashed red line is the first cycle in which the mean effective stress reaches a near-zero value that was introduced earlier as the Sf state. Beyond this cycle, the response is termed to be in the post-liquefaction stage. In this stage, as shown in Figure 1A, the stress path follows almost the same "butterfly" shape, with the mean effective stress p entering and exiting the Sf range at very small levels of mean effective stress. This is associated with a considerable and progressive increase of shear strain amplitude between the third and 23rd cycles, both shown with red lines in Figure 1B. More details about the last loading cycle of this test are illustrated in Figure 2A,B, with focus on what happens in the Sf state of response, where the mean effective stress p falls below a corresponding threshold p_{th} that in this particular case is estimated to be around 10 kPa. The state inside the Sf range for this load cycle corresponds to the marked symbols in the stress path from points A to B and C to D in the increasing and decreasing directions of shear stress, respectively, as shown in Figure 2A. The corresponding shear strains generated in the Sf range of p are denoted by Sf strain γ_{sf}, as shown in Figure 2B. The evolution of γ_{sf} in each half-cycle during the entire cyclic shearing process is presented in Figure 2C. The level of γ_{sf} shows an increase with the number of cycles, presumably towards a saturation level. This implies that the rate of γ_{sf} should reduce with the number of cycles.

Such increasing large shear deformations in the post-liquefaction stage have been observed in different undrained cyclic laboratory configurations such as triaxial,[5,18] torsional,[4,19] and direct simple shear.[17] The observations presented in Figure 2C follow a similar synthesis done by Wang et al[2] on undrained cyclic torsional laboratory tests on Toyoura sand at a D_r=70%. While a considerable level of information can be obtained from such experimental tests, they only include the macroscopic measures of response such as stress, strain, density, and pore pressure. Understanding the mechanical interaction at the particle level is key for explaining the increase of γ_{sf} in undrained cyclic tests. Some meaningful micro-structural measures of the granular assembly such as particle fabric during the course of loading are left unexplored due to the equipment limitations in these physical experiments. In recent years, numerical experiments on idealized particles using DEM have been proven very effective to understand micromechanics behind the complex response of granular material. These methods are used to carry out qualitative studies on granular assemblies to examine the evolution of particle fabric, anisotropy, and other important microscopic quantities during the course of loading. In some recent studies, 2-D DEM simulations on disk particles are used to reproduce shear deformations in the post-liquefaction response. The results have contributed to understanding the constant volume cyclic response of sands from a micromechanical perspec-

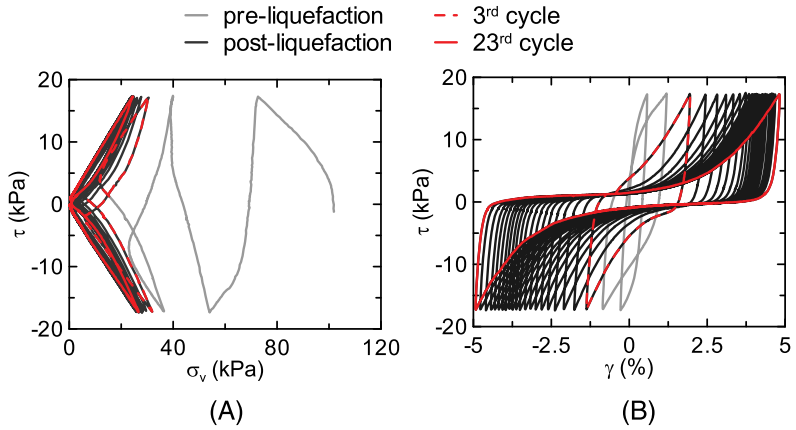

FIGURE 1 Experimental results of an undrained cyclic simple shear test on Ottawa F-65 sand at $D_r = 77\%$: (A) stress-path and (B) stress-strain loops. The red dashed and red continuous lines correspond to the third and 23rd cycle, respectively, encompassing all cycles in the post-liquefaction stage (data from Parra[17])

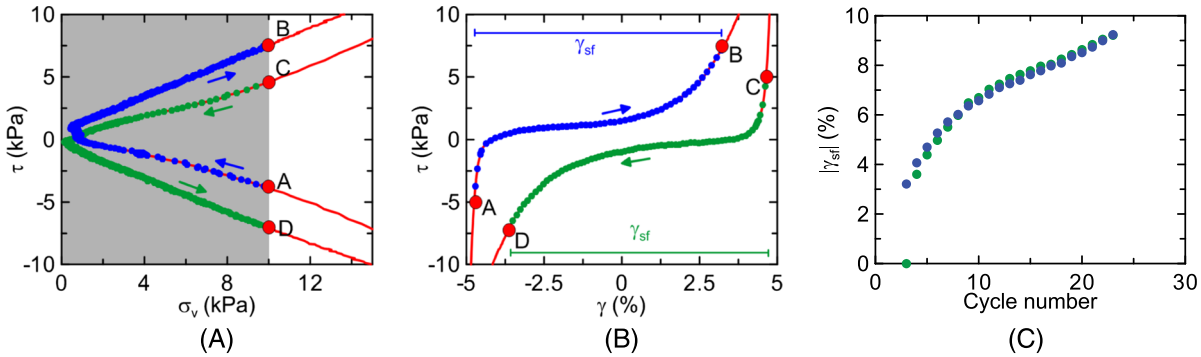

FIGURE 2 Details of shear strain accumulation in the semifluidized state: (A and B) stress-path and the corresponding stress-strain loops in the 23rd loading cycle Figure 1, illustrating the shear strains generated within the semifluidized state, γ_{sf}, while increasing and decreasing the shear stress between points A and B, and points C and D, respectively, and (C) absolute values of the γ_{sf} in the half cycles of all loading cycles

tive. In particular, Wang and Wei[20] used constant volume cyclic biaxial tests to highlight a proposed measure of "centroid difference" for quantifying the geometrical arrangement between particles and the surrounding voids. With a direct correlation between the centroid difference and the level of shear strain amplitude γ, the study suggests that stress-strain loops reach a maximum level of γ that corresponds to the minimum centroid difference. Using the same configuration as in the previous study, Wang et al[2] looked at the average distance of the three closest particles per grain, also known as the mean neighboring particle distance (MNPD), to establish a direct correlation between the maximum level of γ_{sf} and MNPD. These DEM studies have consistently shown that shear strain amplitude increase occurs at low stresses and low coordination number and can be correlated to appropriately defined quantities at grain scale, measured via DEM analysis. Lastly, the value of p_{th} at present cannot be exactly defined because the Sf state reflects a very complex situation. One could for example use such criteria for p_{th} as the value of p when the coordination number falls below the value of 4, observed in 3-D DEM analysis such as in Barrero et al.[21] However, large shear strain could occur for larger values of p; hence, in this paper, the suggestion of $p_{th} = 10$ kPa is a convenient estimate that could eventually change if new evidence is provided, with no consequence on the basic structure of the model.

3 | CONSTITUTIVE MODEL FORMULATION WITHIN THE SF RANGE

3.1 | Reference constitutive model

The reference constitutive model in this study follows the basic premises of the original two-surface plasticity model developed by Manzari and Dafalias[14] and its sequel by Dafalias and Manzari,[11] which formed the basis of what was later on

named SANISAND class of models.[22] The modeling approach follows the framework of bounding surface plasticity with kinematic hardening of the yield surface (YS) and critical state soil mechanics concepts, allowing for a unified description at any pressure and density by the same set of model constants. The SANISAND class includes various extensions.[15,22-25] The earlier works[11,14] represent the core of the constitutive model, and the above-referenced subsequent works build into the model different constitutive features that can be added to the original model framework. To involve fewer model parameters and for simplicity, the version with fabric change effects[11] and an overshooting correction scheme as described in Dafalias and Taiebat[25] has been considered as the reference soil constitutive model, and from here on, it will be referred to as the reference model. Aside from the two overshooting parameters for overshooting correction with default values of $\bar{\varepsilon}^{\mathrm{p}}_{\mathrm{eq}} = 0.01\%$ and $n = 1$, this reference model has 15 parameters listed in Table 1. This version is recently used in a comprehensive study by Ramirez et al.[26] An extensive description of the reference model can be found in the foregoing references, and here a brief descriptive outline of only some relevant constitutive ingredients of the reference model will be presented.

The major constitutive ingredients of the model are the use of bounding and dilatancy surfaces, abbreviated as BS and DS, respectively, in multi-axial deviatoric stress space, generalizing the peak stress ratio and dilatancy stress ratio (phase transformation line slope) in p-q space, respectively. Both surfaces are made functions of the state parameter ψ[27] such that at the critical state, where $\psi = 0$, the surfaces collapse onto the fixed critical state surface that generalizes the critical state stress ratio $q/p = M$ in p-q space. Such dependence of BS on ψ allows the description of the softening response for denser than critical samples, an idea first promoted by Wood et al.[28] But even more important is the dependence of DS on ψ, first introduced by Manzari and Dafalias,[14] because it is the underlying reason why the model can simulate the response of both dense and loose samples with the same set of constants while maintaining compatibility with the premises of critical state theory. Moreover, the model is able to capture the mean effective stress reduction due to the gradual increase of pore water pressure during cyclic loading under undrained conditions, such cyclic loading response is naturally described by means of kinematic hardening. The plastic modulus and dilatancy of the model are controlled by two parameters symbolized by h_0 and A_0, respectively. To better capture the sand response in cyclic loading, the contraction tendency during reverse loading following a dilation phase is enhanced by a fabric-dilatancy tensor, which accounts for the fabric changes during plastic dilation with evidence in microscopic studies. This enhances the pore pressure build-up towards the liquefaction state and allows the model to capture the butterfly shape of the stress path, as observed in the experiments. The model is proven successful in reproducing the monotonic and pre-liquefaction cyclic response of sands for a wide range of pressures and densities.[11,26,29] However, under undrained cyclic simple shear test, the stress-strain loops of the model in the post-liquefaction stage appear to lock-up within a few cycles, preventing it to capture the increase of large cyclic shear strains with the number of cycles as seen in the experiments. This aspect is intended to be improved with the following generic proposed modification.

TABLE 1 Calibrated parameters for reference model

Description	Symbol	Ottawa F-65 Sand[a]	Toyoura Sand[b]
Elasticity	G_0	125	125
	ν	0.33	0.05
Critical state	M	1.26	1.25
	c	0.8	0.712
	λ_c	0.0287	0.019
	e_{ref}	0.78	0.934
	ξ	0.7	0.7
Yield surface	m	0.02	0.02
Plastic modulus	h_0'	4.6	9
	c_h	0.968	0.968
	n^b	2.3	1.25
Dilatancy	A_0'	0.5	0.4
	n^d	2.5	0.7
Fabric dilatancy	$z_{\max}$	25	20
	c_z	500	800

[a] Modified from Ramirez et al.[26]

[b] Modified from Taiebat et al.[29]

3.2 | Proposed modification: The SANISAND-Sf model

The general idea underlying the proposed SANISAND-Sf model is to introduce a small threshold value of mean effective stress p, symbolized by p_{th}, below which the granular assembly is considered to be in a Sf state (hence the acronym Sf in the name of the model), with "very" small plastic modulus and dilatancy ability. By defining the pressure ratio $p_r = p/p_{\text{th}}$, this means that for $p_r < 1$, one should have an increasing amplitude of shear strain in each load cycle that can be attained by decreasing progressively the already small value of the plastic modulus due to small p. This can be achieved by introducing an evolving state internal variable called "strain liquefaction factor (SLF)" symbolized by l which evolves continuously from an initial value (usually 0) to a final saturation value (eg 1), but "only" when $p_r < 1$, ie during the Sf state. This state internal variable will be used for reducing the aforementioned plastic modulus and dilatancy parameters h_0 and A_0 inside this state. The important thing is that the scheme to be used in the range $p_r < 1$ will not significantly affect the response in terms of plastic modulus and dilatancy when we go outside the Sf range, ie the SANISAND-Sf model will resume the response of the reference model by a continuous transition to it.

In order to easily understand the role of the SLF, it is instructive to recall below the analytical expressions of the plastic modulus K_p and dilatancy D of the reference model as follows:

$$K_p = h_0 \left[\frac{2}{3} G_0 (1 - c_h e)(p/p_{\text{at}})^{1/2}\right] \frac{\left(\boldsymbol{\alpha}_\theta^b - \boldsymbol{\alpha}\right) : \boldsymbol{n}}{(\boldsymbol{\alpha} - \boldsymbol{\alpha}_{\text{in}}) : \boldsymbol{n}} \tag{1}$$

$$D = A_0 \left[1 + \langle \boldsymbol{z} : \boldsymbol{n} \rangle\right] \left(\boldsymbol{\alpha}_\theta^d - \boldsymbol{\alpha}\right) : \boldsymbol{n}, \tag{2}$$

where h_0, A_0, G_0, and c_h are model parameters; e and p_{at} are the void ratio and atmospheric pressure, respectively; $\boldsymbol{\alpha}$ is the back stress-ratio tensor; $\boldsymbol{\alpha}_{\text{in}}$ is the initial value of $\boldsymbol{\alpha}$ at the initiation of a new loading process taking place when the denominator of Equation (1) becomes negative according to the rules discussed by Dafalias[30]; $\boldsymbol{\alpha}_\theta^b$ and $\boldsymbol{\alpha}_\theta^d$ are the image back stress-ratio tensors on the bounding and dilatancy surfaces, respectively; $\boldsymbol{n}$ is the loading/unloading direction; and $\boldsymbol{z}$ is the fabric-dilatancy tensor variable. The reader can refer to Dafalias and Manzari[11] for a more comprehensive explanation of the foregoing quantities, while in regards to the present development, the important thing in Equations (1) and (2) is that K_p and D are proportional to the model parameters h_0 and A_0, respectively.

With h_0' and A_0' denoting for the present need the constant parameters that multiply the plastic modulus and dilatancy, respectively, in the reference model, and h_0 and A_0 representing their modified and variable values in the SANISAND-Sf model, the evolving SLF l is then used to modify the ratios h_0/h_0' and A_0/A_0' based on the expressions

$$h_0 = h_0' \left\{\left[1 - \langle 1 - p_r \rangle\right]^{xl} + f_l\right\} \tag{3}$$

$$A_0 = A_0' \left\{\left[1 - \langle 1 - p_r \rangle\right]^{xl} + f_l\right\}, \tag{4}$$

where the Macauley brackets $\langle\ \rangle$ operate according to $\langle A \rangle = A$ if $A > 0$ and $\langle A \rangle = 0$ if $A \leq 0$, while x is a positive model constant, and f_l is a very small number, that are going to be discussed later. After entering the Sf range of $p_r < 1$, the above equations allow h_0 and A_0 to get smaller values than their typical constant values of h_0' and A_0' in the reference model, leading to softer shear modulus and equally softer dilation, hence maintaining the same level of volumetric strain rate. The latter is true because in the reference model, the plastic volumetric strain rate is given by $\dot{\varepsilon}_v^p = D|\dot{\varepsilon}_q^p|$, with $|\dot{\varepsilon}_q^p|$ the absolute value of the plastic deviatoric strain rate, being inversely proportional to plastic modulus, thus to h_0, while D is proportional to A_0; hence, when h_0 and A_0 are obtained by h_0' and A_0' multiplied by the same factor (the term in $\{\}$ in Equations (3) and (4)), the $\dot{\varepsilon}_v^p$ remains the same. The foregoing can straightforwardly be generalized to the multiaxial space where the equivalent plastic shear strain rate substitutes for the triaxial quantity $|\dot{\varepsilon}_q^p|$. The constant f_l is a very small positive number (eg, 0.01 in the present work) and guarantees that h_0/h_0' and A_0/A_0' stay positive at $p = 0$. When $p_r > 1$, given the effect of the Macauley brackets $\langle 1 - p_r \rangle = 0$, Equations 3 and 4 yield values for h_0 and A_0 equal to h_0' and A_0' multiplied by $1 + f_l$, which is very close to 1; this is the reason we opted to maintain the h_0 and A_0 notation as the general one for all p. To the contrary, when $p_r < 1$, the values of h_0 and A_0 reduce significantly as l evolves from 0 to 1 and as p_r tends to 0; when $p_r = 0$, one has that $h_0 = h_0' f_l$ and $A_0 = A_0' f_l$, or when $l = 1$ and $p_r < 1$, one has that $h_0 = h_0' \left\{p_r^x + f_l\right\}$ and $A_0 = A_0' \left\{p_r^x + f_l\right\}$, both scenarios leading to very small positive values. Notice that based on Equation (1), $K_p = 0$ when $p = 0$, irrespective of the value of h_0. This simple modification of the h_0 and A_0 parameters through the newly proposed state internal variable l will guarantee the increasing amplitude of shear strains in the Sf zone in subsequent

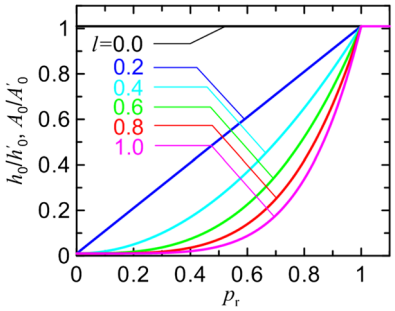

FIGURE 3 Variations of the h_0/h_0' and A_0/A_0' ratios with p_r at different levels of l, illustrating the upper and lower bounds of these ratios in the semifluidized state

cycles as l evolves without altering the response outside the zone. The upper bound of 1 for the variable l will ensure its ultimate saturation, hence that of the strain amplitude. Figure 3 illustrates the variations of h_0/h_0' and A_0/A_0' at different levels of state internal variable l and for different values of p_r. It will be shown subsequently that the x controls the max level of the shear strain amplitude inside the Sf region, and as such, it can be made function of other state variables, for example, relative density D_r. A simple linear expression such as $x = x_0 - c_f D_r$ can be tested with x_0 and c_f two constants. In this work, this important issue that may be more complex than at first thought will not be considered.

We will now address the very important evolution equation for the SLF l. Recall that within the Sf range, the requirement compatible with Equations (3) and (4) is that variable l increases from 0 to 1 during plastic loading. Its value will not affect the response for $p_r > 1$, as already mentioned, but there is an important point to observe. In subsequent loading associated with volume change, the sample consolidates, and if a constant volume cyclic loading begins again after the consolidation, one cannot expect the prior acquired value of l, possibly even $l = 1$, to have a full impact on this subsequent constant volume cyclic loading. It is, therefore, necessary to have a mechanism of restoring the value of l back to its initial value of 0 in a progressive way. Thus, a term of back-to-zero recovery must be added to the evolution rate of l that will operate during drained loading taking place in a reconsolidation after the end of a constant volume cyclic one. In order to address these two requirements for the evolution of l, ie reaching a max value 1, and upon drained (or semi-drained) deformation return to 0, the following rate equation of evolution is proposed:

$$\dot{l} = \langle L \rangle \left[\left(\frac{p_{\text{in}}}{p_{\text{inr}}} \right)^{a} c_l \langle 1 - p_r \rangle (1 - l)^{n_l} \right] - c_r l |\dot{\varepsilon}_{\text{v}}|, \tag{5}$$

where L is the loading index (or plastic multiplier) inside Macauley brackets indicating that the first term of the right-hand side (RHS) operates only when plastic loading occurs. In addition, the $\langle 1 - p_r \rangle$ indicates that this first term can only operate for $p_r < 1$, ie in the Sf state. c_l and n_l are two positive model parameters controlling, respectively, the pace and the nonlinearity of evolution of l towards 1. p_{in} is the mean effective stress at the initiation of a new loading process, with the same criterion of updating as $\boldsymbol{\alpha}_{\text{in}}$ in the reference model, and p_{inr} and a are two positive model constants. To better understand the role of these two parameters, consider the following. In a constant volume cyclic simple shear loading, when the stress path reaches the "locked" butterfly shape of subsequent contraction and dilation phases, depending on the level of cyclic shear stress amplitude, p_{in} attains a certain value at the reversal points. The corresponding value of p_{in} in a test with a selected "reference" cyclic shear stress can be considered as p_{inr}. Based on this p_{inr}, the parameter a will influence the rate $\dot{l}$ in other levels of cyclic shear stress. The above argument is directly applicable to undrained cyclic simple shear loading in which the locked stress path is almost symmetric. Other cyclic shearing scenarios that are associated with asymmetric locked stress paths, eg cyclic triaxial shearing, have two different levels of p_{in} in each cycle. Furthermore, for random cyclic loading, p_{in} acquires different values along with $\boldsymbol{\alpha}_{\text{in}}$ at the initiation of new loading processes. In those cases, the above two parameters still play the same role, and it is hoped and expected that this role will be similarly effective under these more general loading processes as it was under almost symmetric cyclic shearing. This is of course typical of the calibration of any constitutive model parameter from a specific loading data, expected to be appropriate for more general loading conditions.

The second term of the RHS in Equation (5) with the model constant c_r provides the return-to-zero of l in any loading scenario where $|\dot{\varepsilon}_{\text{v}}| \neq 0$, ie when drainage and reconsolidation occur, with $\dot{\varepsilon}_{\text{v}}$ being the total volumetric strain rate. The absolute value of $\dot{\varepsilon}_{\text{v}}$ was introduced in order to exclude the possibility of increasing the value of l above 1 in case the

drained deformation that may involve shearing induces dilation (negative value of $\dot{\varepsilon}_v$). The existence of l itself in the second term of the RHS guarantees that once $l = 0$, it stays at zero until the first term of the equation is activated again when $1 - p_r > 0$ inside the Sf range. Then, the evolution of l towards 1 takes place and is not affected by the second term of the RHS of Equation (5) during undrained loading because $\dot{\varepsilon}_v = 0$.

Notice that if drained loading takes place at very small values of p such that $1 - p_r > 0$, both terms of Equation (5) are active with a competing simultaneous evolution of l towards 1 (first term) or 0 (second term), which, however, cannot move outside its range from 0 to 1 under any circumstances. Such a drained loading at very small p is rather unusual and has no serious effect in any case. In this work, we will be dealing exclusively with simulations of undrained cyclic loading, hence the second return-to-zero term of the RHS of Equation (5) will be inactive. Nevertheless, a preliminary qualitative investigation without comparison with experimental data will be conducted on the effect of return-to-zero term in Equation (5) and accordingly on the ensuing calibration process of the related parameter c_r.

4 | CALIBRATION AND PERFORMANCE OF THE NEW MODEL

Considering the foregoing modifications, the new model has two sets of additional parameters: a set of five parameters listed in Table 2 that require detailed calibration and for which sensitivity analysis is carried out and a set of three parameters listed in Table 3 that are set to default values in absence of detailed data. Details of the calibration process including the effects of the calibrated additional parameters of the new model are presented in this section, followed by the performance of the SANISAND-Sf model compared with a number of different tests.

The performance of the proposed model is evaluated by the success of the simulation of five undrained cyclic simple shear tests on Ottawa F-65 sand by Parra[17] and one undrained cyclic torsional test on Toyoura sand by Zhang.[31] The selected undrained cyclic simple shear tests on Ottawa F-65 sand were carried out at an initial vertical effective stress $\sigma_v \simeq 100$ kPa and a relative density of $D_r \simeq 80\%$. The selected undrained cyclic torsional test on Toyoura sand was carried out on an initial mean stress $p \simeq 100$ kPa and a relative density of $D_r \simeq 70\%$.

For the Ottawa F-65 sand, the reference model parameters are adopted from the calibration of Ramirez et al[26] based on an extensive database of monotonic and cyclic shear tests on Ottawa sand. Some of the parameters such as ν, h_0', and A_0' are adjusted from the previous calibration to better represent the response for the experiments on the specific batch of Ottawa F-65 sand by Parra.[17] The fabric dilatancy tensor z_{max} is also modified to bring the stress path near the origin to better address the intended concept of the Sf state in the present study. As for Toyoura sand, the reference model parameters are adopted from Taiebat et al.[29] Parameters such as h_0', A_0', n^d, and z_{max} are again modified to better reproduce the experiments on the specific batch of Toyoura sand by Zhang.[31] The results of the above calibration for the reference model are shown in Table 1.

Using the calibrated parameters of the reference model for Ottawa F-65 sand, and setting the additional parameters p_{th}, f_l, and n_l at their default values shown in Table 3, the effects of the remaining five additional parameters that require calibration were evaluated in simulating one of the target undrained cyclic simple shear tests. The results were illustrated through a number of sensitivity analyses in Section 4.1. Then, based on the calibrated/optimized values of these five parameters, the simulation of the modified SANISAND-Sf model is compared with that of the reference model and

TABLE 2 Calibrated additional parameters of the new model

Parameter	Sensitivity Analysis[c]	Ottawa F-65 Sand	Toyoura Sand
x	4, **5**, 6	5.4	4
c_l	100, **200**, 300	220	50
p_{inr}	25 kPa	25 kPa	45 kPa
a	**0**, 2, 4, 8	8	0[d]
c_r	0, **250**, 1000	0[e]	0[e]

[a]Common values for different sensitivity analyses are shown in bold.

[b]To be calibrated upon availability of data for different levels of CSR.

[c]To be calibrated upon availability of detailed data for multiple-liquefaction stages.

TABLE 3 Default additional parameters of the new model

Parameter	Default Value
p_{th}	10 kPa
f_l	0.01
n_l	8

the experimental data for this test and presented in Section 4.2. This is followed by the simulation of the remaining tests on Ottawa F-65 sand and Toyoura sand with the modified model and comparing the results with the corresponding experimental data.

4.1 | Effects of the new model parameters

Assuming an initial vertical effective stress of $\sigma_{v,0} = 102$ kPa, an initial lateral effective stress of $\sigma_{h,0} = 51$ kPa, and an initial void ratio of $e = 0.58$ (equivalent to $D_r = 77\%$ for Ottawa F-65 sand), a number of sensitivity analyses were carried out on simulation of an undrained cyclic simple shear loading with cyclic stress ratio (CSR) = $\tau_{cyc}/\sigma_{v,0}$=0.174. The reference model parameters for these simulations were those of Ottawa F-65 sand listed in Table 1. The additional parameters of the new model that require calibration, ie x, c_l, c_r, and a, were examined in a number of sensitivity analyses with the values listed in Table 2. The default model parameter were listed in Table 3.

Figures 4 to 6 show results of the sensitivity analyses on the effects of x, c_l, and c_r, respectively, and Figure 7 summarizes these sensitivity analyses. Three different values were used for each of these target parameters in each figure while keeping all other parameters constant. The simulations continued until reaching $l = 0.6$. Results are presented in terms of shear strain γ, shear stress τ, strain liquefaction factor l, absolute value of the Sf shear strain $|\gamma_{sf}|$, and the number of cycles.

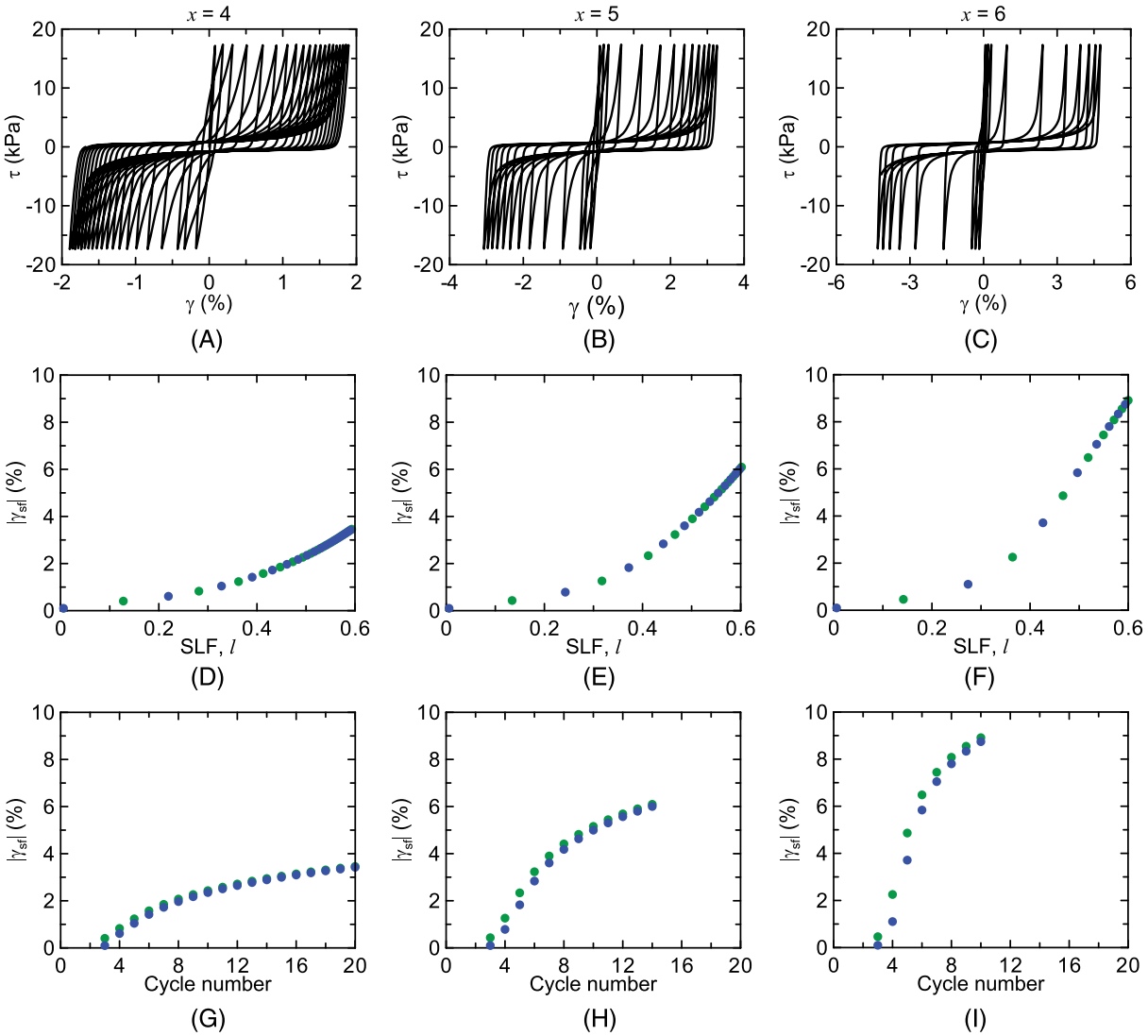

FIGURE 4 Illustration of the effect of x on the maximum amplitude of post-liquefaction shear strain, in simulation of undrained cyclic simple shear loading: (A-C) stress-strain loops, (D-F) evolution of γ_{sf} with the strain liquefaction factor up to $l = 0.6$, and (G-I) evolution of the γ_{sf} with the number of loading cycles

Before going to details of the sensitivity analysis results, let us recall that the increase of the shear strain amplitude in the post-liquefaction stage, which is governed by the reduced shear stiffness in each cycle in the Sf state, is linked to the evolved value of l. As l evolves from 0 and tends to values closer to 1, the amplitude of post-liquefaction shear strain appears to saturate towards a maximum value. The actual maximum value of γ_{sf} is only achieved when $l = 1$. It would take a lot more cycles than what is shown in these figures to actually reach $l = 1$; however, the presented simulation results show that even at $l = 0.6$, the γ_{sf} starts to approaching its saturation level.

Figure 4A-C shows that x has a direct relation to this maximum value, as x increases, the maximum attained level of post-liquefaction shear strain amplitude also increases. This can also be clearly observed in Figure 4D,F that for $x = 4$, 5, and 6, at $l = 0.6$, we reach $\gamma_{sf} \simeq 3.5\%$, 6%, and 9%, respectively; these are summarized in Figure 7A to highlight the effect of parameter x. In fact, in each case of x, this figure shows the developed $|\gamma_{sf}|$ for different attained levels of l from 0 to 0.6. Figure 4G-I shows that with lower levels of x, it takes more number of cycles to reach $l = 0.6$ than for higher levels of x. The pace of evolution for the strain liquefaction factor l is controlled by the model parameter c_l. Figure 5A,C shows an inverse relation between the value of c_l and the pace of evolution of the post-liquefaction shear strain toward its saturation level, ie, as c_l increases, the pace of evolution of γ_{sf} decreases. For these three simulations, the same level of $x = 5$ is used, hence as expected at $l = 0.6$, all three cases reach the same post-liquefaction shear strain amplitude, or the same $\gamma_{sf} \simeq 6\%$ as shown in Figure 5d to 5f. The effect of parameter c_l in the pace of evolution of the Sf shear strain can

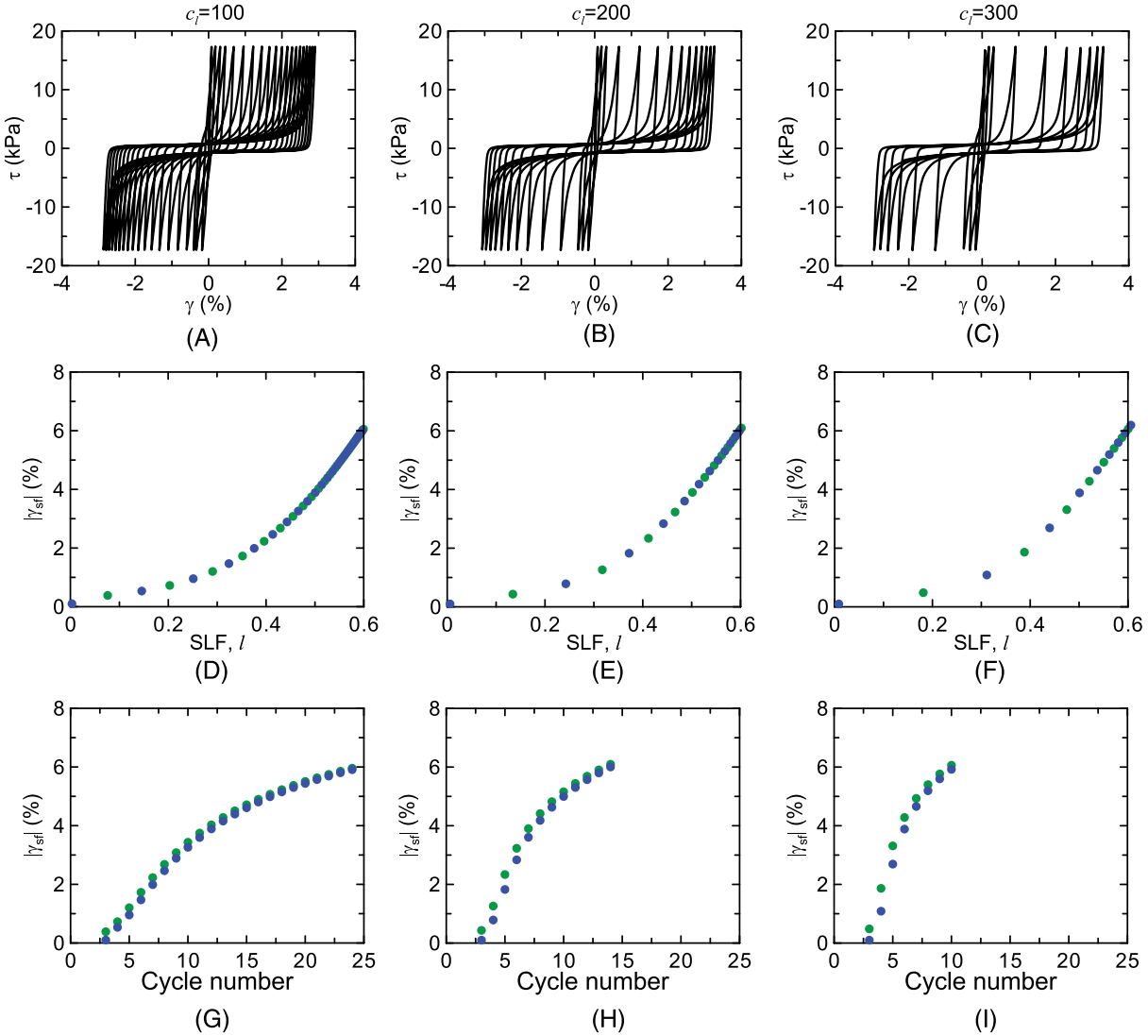

FIGURE 5 Illustration of the effect of c_l on the pace of evolution of post-liquefaction shear strain amplitude towards its saturation level, in simulation of undrained cyclic simple shear loading: (A-C) stress-strain loops, (D-F) evolution of γ_{sf} with the strain liquefaction factor up to $l = 0.6$, and (G-I) evolution of the γ_{sf} with the number of loading cycles

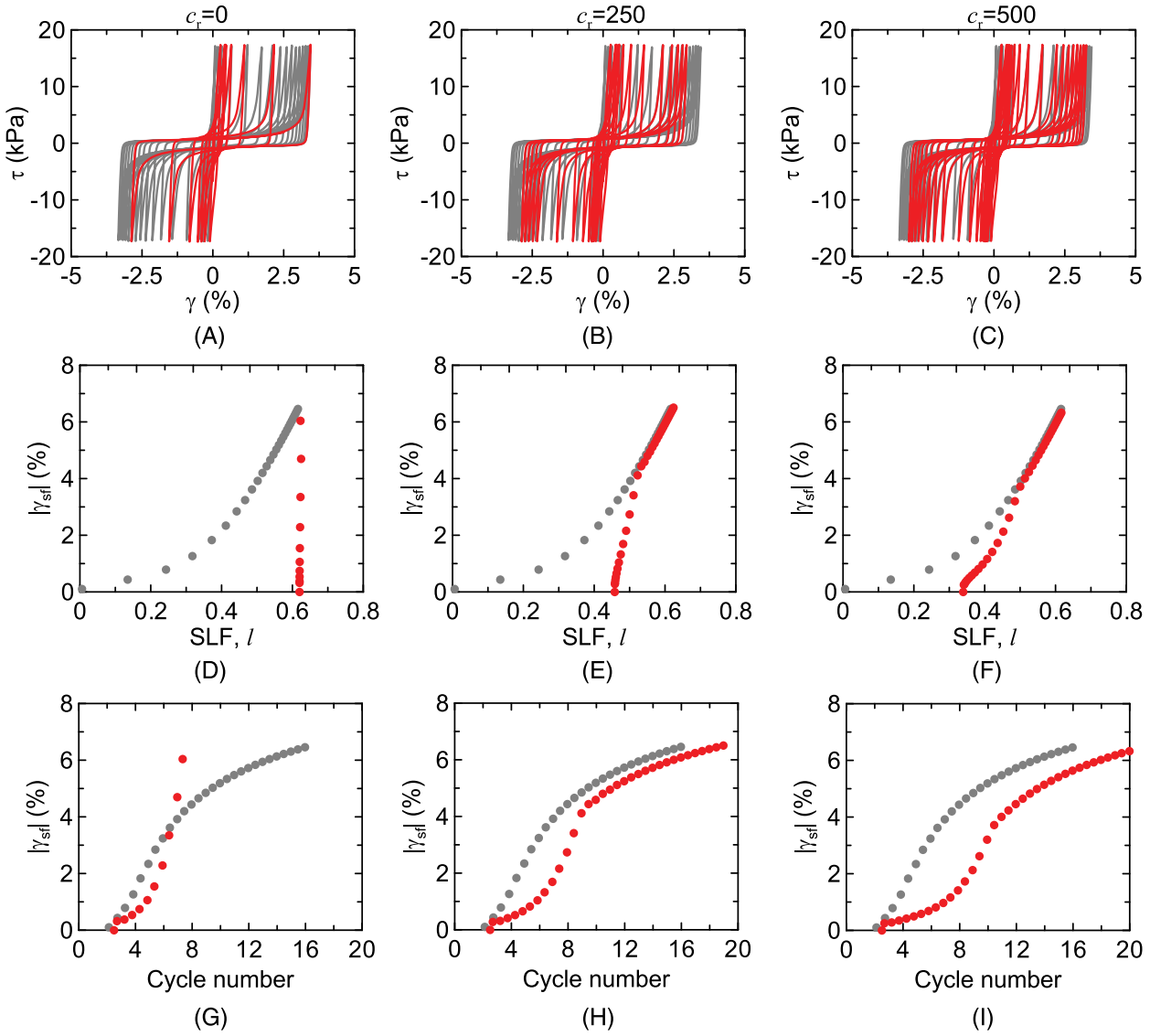

FIGURE 6 Illustration of the effect of c_r on the post-liquefaction response after a drained reconsolidation stage, where the first undrained cyclic shearing is shown in grey and the second undrained cyclic shearing is shown in red: (A-C) stress-strain loops, (D-F) evolution of γ_{sf} with the strain liquefaction factor up to $l = 0.6$, and (G-I) evolution of the γ_{sf} with the number of loading cycles

also be clearly observed in Figure 5G-I such that the cases of $c_l = 100$, 200, and 300 reach the $\gamma_{sf} \simeq 6\%$, in 23, 14, and 10 cycles, respectively; these are summarized in Figure 7B to clearly highlight the effect of parameter c_l. Again, in each case of c_l, this figure shows the developed $|\gamma_{sf}|$ for different attained levels of l from 0 to 0.6. More specifically, Figure 7A,B summarize the key observations from the sensitivity analyses on x and c_l. Although both of these parameters affect in a synergistic way the features of the post-liquefaction cyclic shear strain response, each one plays a predominant role in regards to one of these features, guiding its calibration process: x controls the maximum amplitude of γ_{sf} and c_l controls the number of cycles in the post-liquefaction stage before reaching the maximum amplitude of γ_{sf}.

To address the way to go about calibrating the return-to-zero parameter c_r, Figure 6 shows three sets of simulations with different values for c_r. In these simulations, undrained cyclic simple shear loading leads to a first liquefaction round and brings SLF to $l = 0.6$ as shown with grey symbols in Figure 6D-F. It takes around 16 cycles of shearing to reach this level of l, and at this state, the double amplitude shear strain reaches around 7% (see grey symbols in Figure 6G-I). This is followed by a drained reconsolidation stage to bring the vertical effective stress back to its initial value. Using different levels of c_r in this stage of loading leads to different levels of recovery of l. The corresponding path of return of l to smaller values is not shown in the figure. This is again followed by another undrained cyclic shearing to a second liquefaction round and bringing SLF from its returned value at the end of the drained reconsolidation stage again to $l = 0.6$, as shown with red

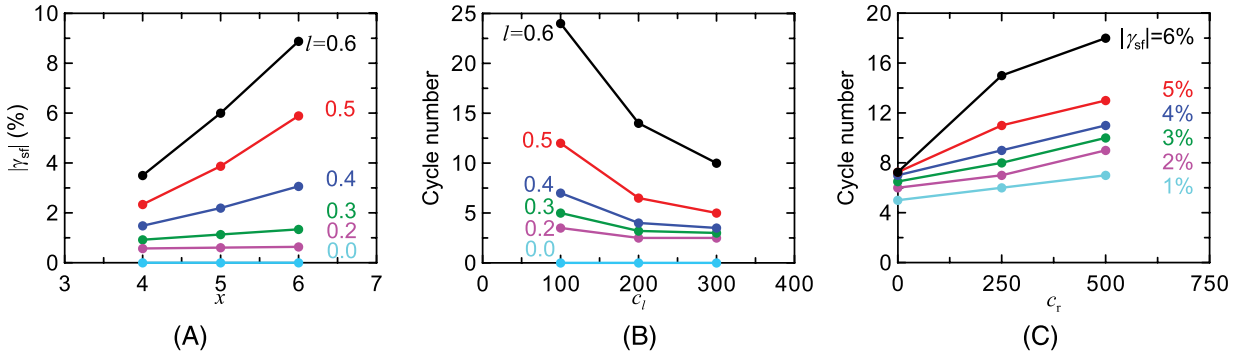

FIGURE 7 Summary of the effects of x, c_l, and c_r on different aspects of the post-liquefaction response from Figures 4 to 6: (A) effect of x on the attained values of $|\gamma_{sf}|$ at different levels of l, (B) effect of c_l on the number of cycles to reach different levels of l, and (C) effect of c_r on the number of cycles to reach different levels of $|\gamma_{sf}|$ in the second liquefaction round

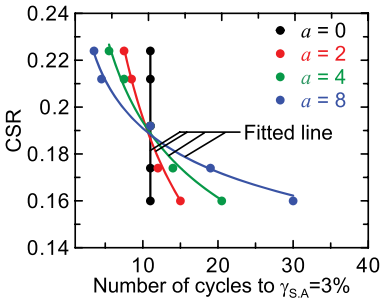

FIGURE 8 Illustration of the effect of a on the number of cycles to reach 3% of single amplitude shear strain ($N_{\gamma_{SA}=3\%}$) in simulation of undrained cyclic simple shear loading with different level of cyclic stress ratio (CSR)

symbols in Figure 6D-F. At this state, the double-amplitude shear strain almost reaches again to the same level of 7% as in the first liquefaction round. The stress-strain loops and the corresponding evolutions of l, γ_{sf}, number of cycles for the first and second undrained shearing rounds and the corresponding post-liquefaction response are presented in different rows of Figure 6. $c_r = 0$ represents the scenario where the back-to-zero recovery mechanism of SLF is inactive and therefore l remains at 0.6. In this case, it takes only around seven cycles in the second round to reach the 7% double-amplitude shear strain. For the cases of $c_r = 250$ and 500, the SLF recovers during the drained reconsolidation stage to the values 0.46 and 0.34, respectively. As a result of this, the corresponding number of cycles in the second round to reach the 7% double amplitude of shear strain are 19 and 20. The higher the c_r, the faster the pace of recovery of l, and the greater number of cycles to reach the same level of shear strain in the post-liquefaction of the second round compared with the first round. The outcomes of the sensitivity analysis on c_r are summarized in Figure 7c for reaching different levels of $|\gamma_{sf}|$. This figure, in fact, elaborates on the constitutive role of the back-to-zero recovery parameter c_r and shows a systematic way for calibration of this parameter provided that such type of experimental data becomes available.

The slope of plots of CSR vs number of cycles to reach a certain value of shear strain in the post-liquefaction stage (CSR-N) can be controlled using parameters p_{inr} and a. These parameters directly influence the term $(p_{in}/p_{inr})^a$ in Equation (5) and therefore the rate of evolution of l in the Sf state. The effect of this term is elaborated in Figure 8 for the plot of CSR vs number of cycles to reach 3% of the single-amplitude shear strain ($N_{\gamma_{SA}=3\%}$). Here, for $p_{inr} = 25$ kPa, the parameter a has been varied from 0, which is equivalent to $(p_{in}/p_{inr})^a = 1$ hence no effect of this term in $\dot{l}$, to 8 that is equivalent to different levels of $(p_{in}/p_{inr})^a$ depending on the CSR. In general, for a nonzero value of a, the lower the CSR, the higher the $N_{\gamma_{SA}=3\%}$. The slope of CSR-N becomes milder at higher values of a.

Parameter p_{th} was set at a default value of 10 kPa. Sensitivity analysis (not shown here) reveals that the value of p_{th} controls the minimum thickness of the cyclic shear stress-strain loops. It is believed that the value of p_{th} should be very small; however, a default value of 10 kPa appears to provide reasonable results as shown in the next section.

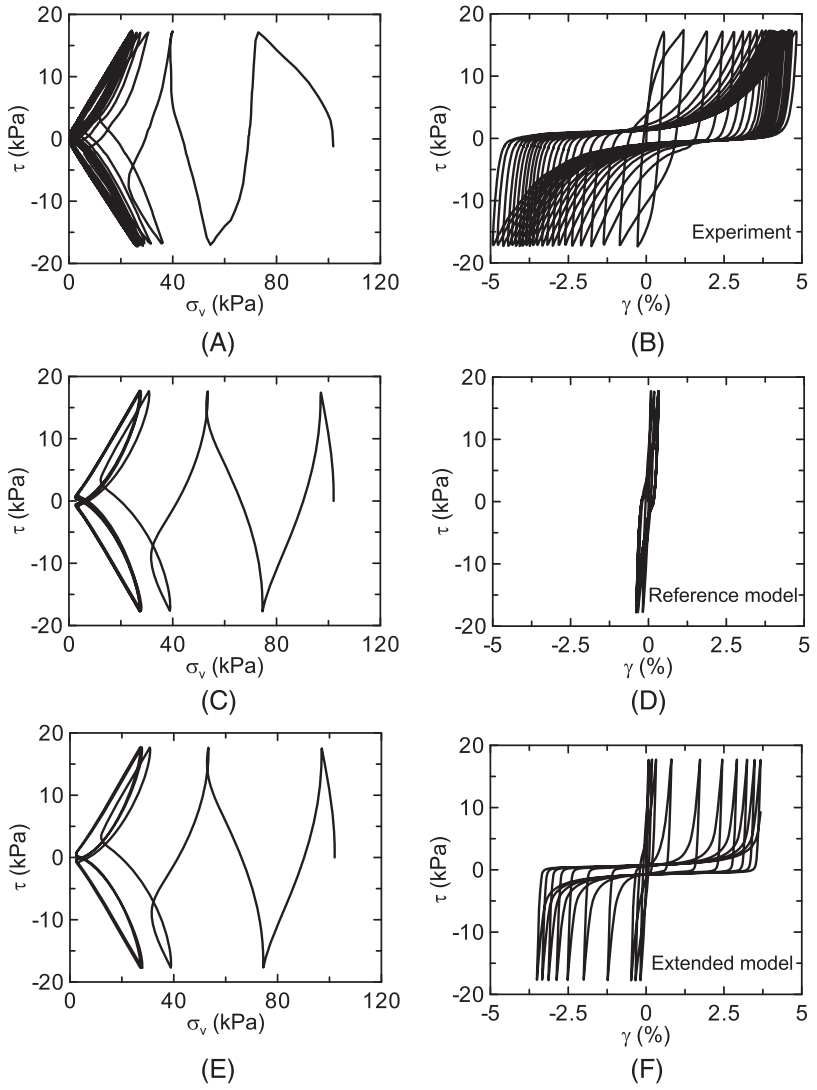

FIGURE 9 Stress-path and stress-strain loops of an undrained cyclic simple shear test on Ottawa F-65 sand at $D_r = 77\%$: (A nd B) experimental results from Parra,[17] (C and D) reference model simulation results, and (E and F) extended model accounting for semifluidized strains

4.2 | Simulation of undrained cyclic response on Ottawa F-65 and Toyoura sand

Based on the trends obtained in the sensitivity analyses of the previous section, the additional parameters of the new model that require calibration were optimized for the data of Ottawa F-65 sand[17] using a trial-and-error process. For this purpose, given the corresponding experimental data of undrained cyclic simple shear tests with CSR= 0.174 as shown in Figure 9A,B, and more specifically with reference to the stress-strain loops shown in Figure 9B, x and c_l were calibrated to 5.4 and 220, respectively. Recalling the combined role that parameters p_{inr} and a play in the term $(p_{\text{in}}/p_{\text{inr}})^a$ that affects the pace of evolution of SLF in Equation (5), the calibrated value of parameter a depends on the choice of parameter p_{inr} that is a selected reference value of the mean effective stress at the reversal point of the stress path in the corresponding locked butterfly loop. Based on $p_{\text{inr}} = 25$ kPa, the post-liquefaction strains at a different level of CSR for this sand are best captured using $a = 8$. Finally, the c_r parameter is set to zero as we don't have data of multiple liquefaction tests on this soil.

Based on the model parameters presented in Tables 1 to 3, results of the undrained cyclic simple shear test on Ottawa F-65 sand at initial vertical effective stress of 102 kPa and relative density of 77% as shown in Figure 9A,B are compared with the corresponding simulation results using the reference model as shown in Figure 9C,D and those from the new model accounting for the Sf state as shown in Figure 9E,F. While both simulations show a similar level of performance in the pre-liquefaction state and in the overall stress path, the new model shows a very clear improvement in capturing the accumulation of shear strain amplitudes in the post-liquefaction cycles as it tends towards a saturated level. Moreover, the

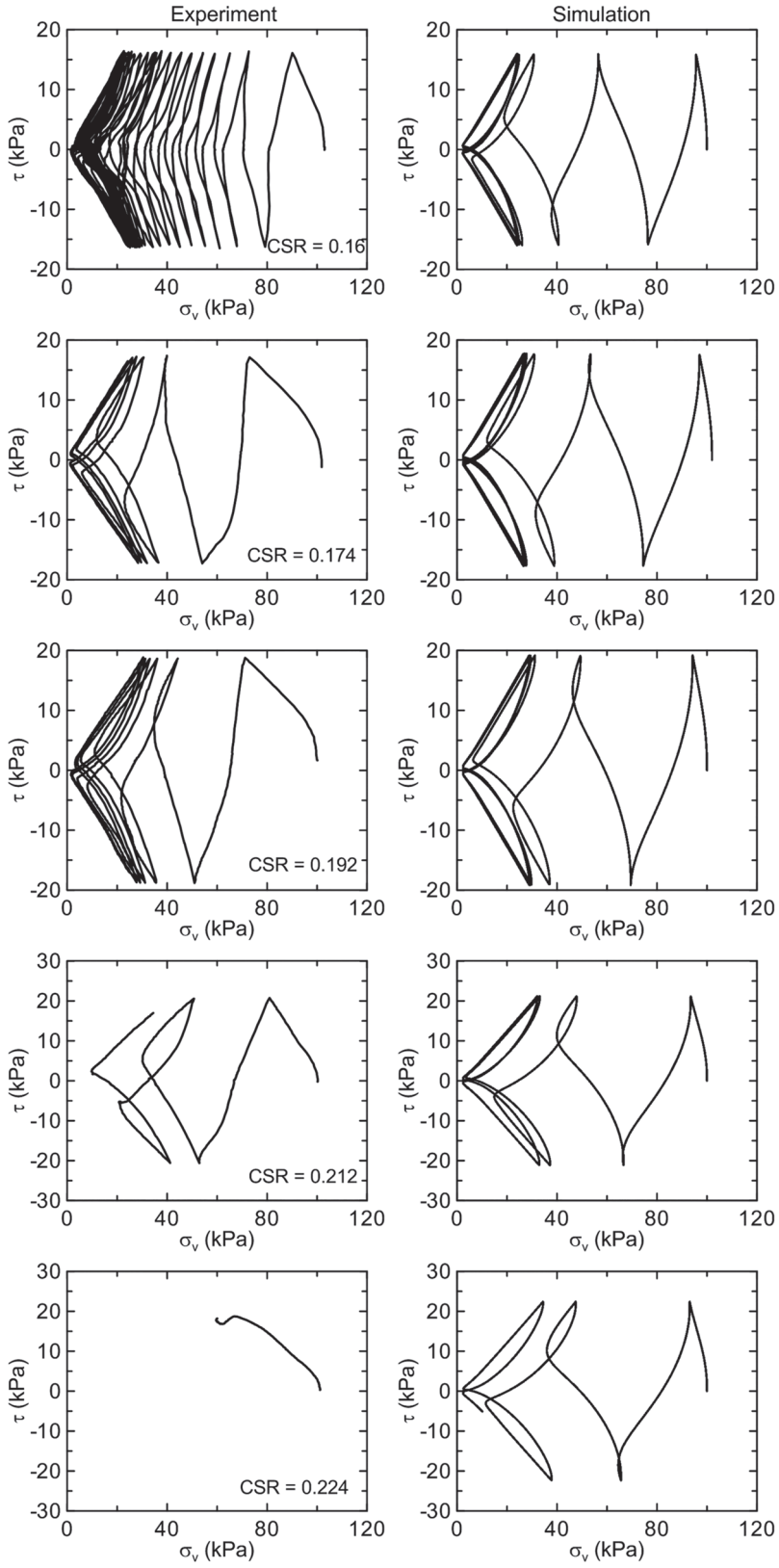

FIGURE 10 Stress-path for different cyclic stress ratio (CSR) levels on undrained cyclic simple shear test on Ottawa F-65 sand at $D_r = 77\%$: experimental and extended model results, data from Parra[17]

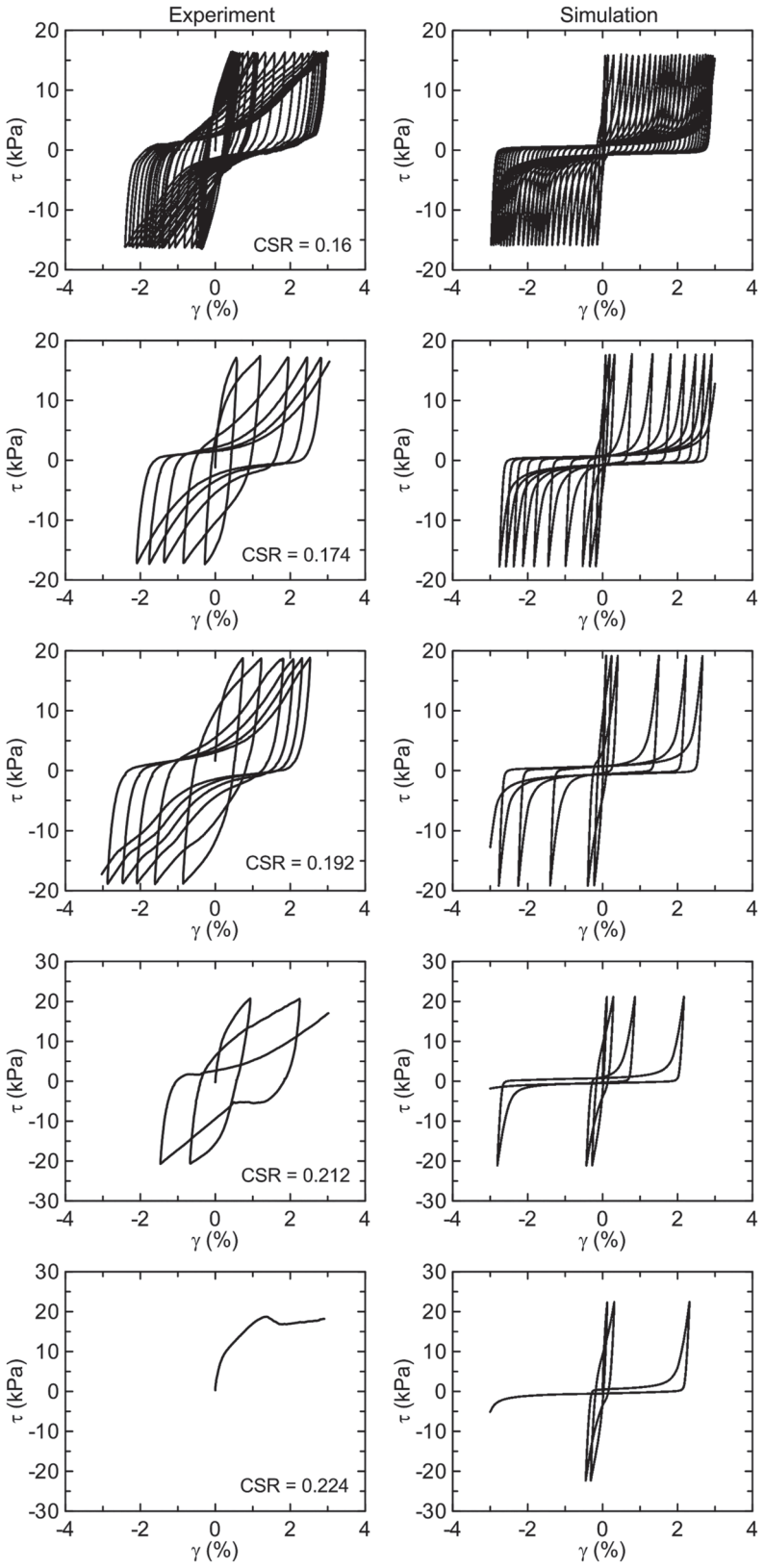

FIGURE 11 Stress-strain loops for different cyclic stress ratio (CSR) levels on undrained cyclic simple shear test on Ottawa F-65 sand at $D_r = 77\%$: experimental and extended model results, data from Parra[17]

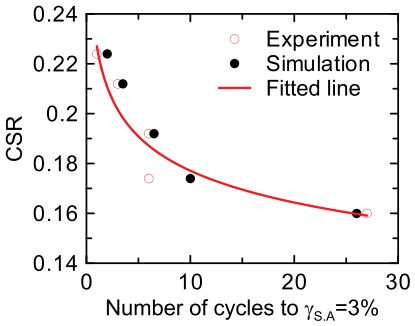

FIGURE 12 Comparing the experimental results and model simulations in terms of cyclic stress ratio versus number of loading cycles to reach 3% single amplitude of shear strain in undrained simple shear tests on Ottawa sand F-65 sand at D_r =77%

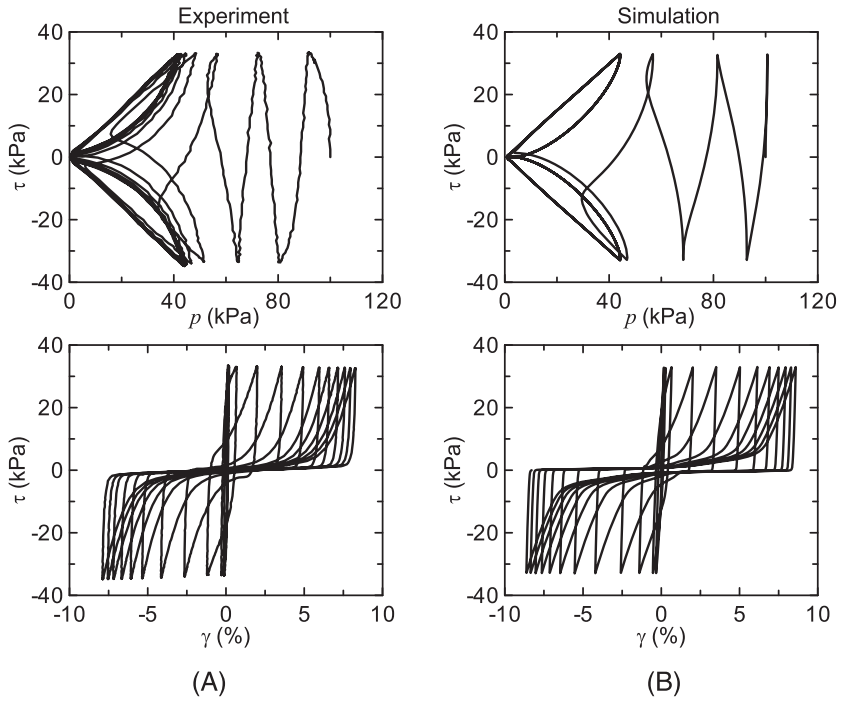

FIGURE 13 Stress-path and stress-strain loops of an undrained cyclic torsional shear test on Toyoura sand at D_r = 70%: (A) experimental results from Zhang[31] and (B) extended model accounting for semifluidized strains

performance of the new model is compared with the experiments at various shear stress amplitudes until reaching 3% of single-amplitude shear strain in Figures 10 and 11. The corresponding results of CSR versus $N_{\gamma_{SA}=3\%}$ are summarized in the CSR-N plot in Figure 12; the level of match between the experiments and the simulations in this plot is an indication of the success of the proposed modification. It should be noted that the reference model cannot even reach the $\gamma_{SA} = 3\%$ in any of these CSR levels, as the stress-strain loops get locked at smaller levels of shear strain.

The performance of the introduced SANISAND-Sf model is also examined by simulating an undrained cyclic torsional test on Toyoura sand at initial mean effective stress of 100 kPa and relative density of 70% by Zhang,[31] as shown in Figure 13. The related model parameters are again listed in Tables 1 to 3. The model shows an excellent performance in capturing both the pre-liquefaction and post-liquefaction response of this test. Note that the parameters a and c_r were set to 0 in the simulation of this test; however, upon the availability of data for different levels of CSR and multiple-liquefaction tests, these parameters can be calibrated to their representative values.

5 | CONCLUSION

Post-liquefaction constant volume cyclic shearing response of sands is associated with a considerable and progressive increase of shear strain amplitudes. This response is linked to reduced plastic shear modulus and dilation tendency in

the semifluidized (Sf) state at low levels of mean effective stress. A new state internal variable named strain liquefaction factor is introduced that evolves from 0 to 1 within the Sf range of low mean effective stresses; its constitutive role is to reduce the values of parameters controlling the plastic modulus and dilatancy, maintaining the same plastic volumetric strain rate, in the Sf range. The evolution rate equation of the strain liquefaction factor includes a back-to-zero recovery term under drained loading, which allows the process of its progressive influence on shear strain amplitude to be repeated upon resuming cyclic loading after drainage. Although not examined in detail, this is a much sought after constitutive feature that is absent from other constitutive models that address the issue of increasing cyclic shear strain amplitude under constant volume loading by permanently decreasing the stiffness by means of an ever increasing function, usually of cumulative shear strain. This new constitutive ingredient of the strain liquefaction factor is added to a reference-bounding surface sand plasticity model[11] which is the precursor of the SANISAND family of models that has proven success in the simulation of monotonic and cyclic response of sand in the pre-liquefaction state. Consequently, the name SANISAND-Sf was introduced for the new model indicating by the initials Sf the consideration of the response in the Sf state.

The new model has two sets of additional parameters: the ones that require calibration and the ones that can be set at default values. Each parameter has been identified to be responsible for certain particular characteristic of response that helps its calibration. Performance of both the reference model and the SANISAND-Sf model are then assessed in the simulation of the stress-path and stress-strain response of an undrained cyclic simple shear test on Ottawa F-65 sand. While the reference model fails in capturing the progressive increase of shear strain amplitudes in the post-liquefaction stage, this important aspect of response has significantly improved in the new extended model. Additional simulations have shown the successful performance of the new model in simulation of stress-strain response of more undrained cyclic simple shear tests on Ottawa F-65 sand and an undrained cyclic simple torsional shear test on Toyoura sand. Nevertheless, one must observe that while the overall fitting of the CSR-N curve is satisfactory, this is often achieved by balancing the under and over prediction of N in the pre- and post-Sf range, respectively. The ideal action would be to have separate satisfactory simulations of the CSR-N curves for these two ranges, and this will be a subject for future investigation.

Sand is a granular media with no viscous effects like clays, but when it reaches the Sf state, it is expected that rate sensitivity of this intermediate between solid and fluid material phase will appear. Nevertheless, some preliminary investigation by means of DEM have shown that the rates required for the mechanical response to exhibit noticeable rate sensitivity are much larger than those typically encountered under cyclic loading. Thus, it is believed that the rate independence assumed also during the Sf state is a realistic assumption.

Further detailed and targeted experimental or DEM studies might suggest several improvements in the proposed formulation for the role and evolution of the newly proposed state internal variable l. In particular, having defined the specific effect of each one of the introduced new parameters on the response within the Sf range, new data may guide their dependence on relative density, initial pressure, and amplitude of the shear stress. In addition, DEM investigations can offer a better understanding of the return-to-zero formulation of the strain liquefaction factor, as proposed in Equation 5, during the consolidation stage of loading between different cyclic liquefaction events. A final note is that the ideas presented by Equations (5) and (4) are generic in concept and do not apply only to the reference model but to any model that has expressions for plastic modulus and dilatancy multiplied by coefficients like h_0 and A_0.

ACKNOWLEDGEMENTS

A.R. Barrero and M. Taiebat acknowledge support by the Natural Sciences and Engineering Research Council of Canada (NSERC) and SRK Consulting. Y.F. Dafalias acknowledges support by the European Research Council under the European Union's Seventh Framework program (FP7/2007-2013)/ERC IDEAS Advanced Grant Agreement 290963 (SOMEF), and the General Secretariat for Research and Technology of Greece (Matching Funds Program) under the project titled SOFI - SOil Fabric Investigation, and partial support by NSF project CMMI-1162096.

ORCID

Mahdi Taiebat https://orcid.org/0000-0003-2067-8161

REFERENCES

1. Kramer SL. *Geotechnical Earthquake Engineering*. Upper Saddle River, New Jersey: Prentice Hall, Inc.; 1996.
2. Wang R, Fu P, Zhang JM, Dafalias YF. DEM study of fabric features governing undrained post-liquefaction shear deformation of sand. *Acta Geotechnica*. 2016;11(6):1321-1337.

3. Seed B, Lee KL. Liquefaction of saturated sands during cyclic loading. *J Soil Mech Found Div*. 1966;92(SM6):105-134.
4. Zhang JM, Wang G. Large post-liquefaction deformation of sand, part I: physical mechanism, constitutive description and numerical algorithm. *Acta Geotechnica*. 2012;7(2):69-113.
5. Rouholamin M, Bhattacharya S, Orense RP. Effect of initial relative density on the post-liquefaction behaviour of sand. *Soil Dyn Earthq Eng*. 2017;97(Supplement C):25-36.
6. Zienkiewicz O, Mroz Z. Generalized plasticity formulation and applications to geomechanics. *Mech Eng Mater*. 1984;44(3):655-680.
7. Pastor M, Zienkiewicz OC, Chan AHC. Generalized plasticity and the modelling of soil behaviour. *Int J Numer Anal Meth Geomech*. 1990;14(3):151-190.
8. Von Wolffersdorff PA. A hypoplastic relation for granular materials with a predefined limit state surface. *Mech Cohesive-frict Mater*. 1996;1(3):251-271.
9. Niemunis A, Herle I. Hypoplastic model for cohesionless soils with elastic strain range. *Mech Cohesive-frict Mater*. 1997;2(4):279-299.
10. Elgamal A, Yang Z, Parra E. Computational modeling of cyclic mobility and post-liquefaction site response. *Soil Dyn Earthq Eng*. 2002;22(4):259-271.
11. Dafalias YF, Manzari MT. Simple plasticity sand model accounting for fabric change effects. *J Eng Mech*. 2004;130(6):622-634.
12. Andrianopoulos KI, Papadimitriou AG, Bouckovalas GD. Explicit integration of bounding surface model for the analysis of earthquake soil liquefaction. *Int J Numer Anal Meth Geomech*. 2010;34(15):1586-1614.
13. Boulanger R, Ziotopoulou K. Formulation of a sand plasticity plane-strain model for earthquake engineering applications. *Soil Dyn Earthq Eng*. 2013;53:254-267.
14. Manzari MT, Dafalias YF. A critical state two-surface plasticity model for sands. *Géotechnique*. 1997;47(2):255-272.
15. Li X, Dafalias Y. Dilatancy for cohesionless soils. *Geotechnique*. 2000;50(4):449-460.
16. Wang R, Zhang JM, Wangm G. A unified plasticity model for large post-liquefaction shear deformation of sand. *Comput Geotechn*. 2014;59:54-66.
17. Parra Bastidas AM. Ottawa F-65 sand characterization. *PhD Thesis*: University of California, Davis, Davis, CA. USA; 2016.
18. Wichtmann T, Triantafyllidis T. An experimental database for the development, calibration and verification of constitutive models for sand with focus to cyclic loading: part I—tests with monotonic loading and stress cycles. *Acta Geotechnica*. 2016;11:739-761.
19. Wahyudi S, Kosek iJ, Sato T, Chiaro G. Multiple-liquefaction behavior of sand in cyclic simple stacked-ring shear tests. *Int J Geomech*. 2015;16(5):C4015001.
20. Wang G, Wei J. Microstructure evolution of granular soils in cyclic mobility and post-liquefaction process. *Granul Matter*. 2016;18(3):51.
21. Barrero A, Oquendo W, Taiebat M, Lizcano A. Cyclic shearing response of granular material in the semi-fluidized regime. *Proceedings of Geotechnical Earthquake Engineering and Soil Dynamics V: Numerical Modeling and Soil Structure Interaction (GSP 292)*. Reston, VA: American Society of Civil Engineers; 2018:100-107.
22. Taiebat M, Dafalias YF. SANISAND: simple anisotropic sand plasticity model. *Int J Numer Anal Meth Geomech*. 2008;32(8):915-948.
23. Dafalias YF, Papadimitriou AG, Li XS. Sand plasticity model accounting for inherent fabric anisotropy. *J Eng Mech*. 2004;130(11):1319-1333.
24. Li XS, Dafalias YF. Anisotropic critical state theory: role of fabric. *J Eng Mech*. 2012;138(3):263-275.
25. Dafalias YF, Taiebat M. SANISAND-Z: zero elastic range sand plasticity model. *Géotechnique*. 2016;66(12):999-1013.
26. Ramirez J, Barrero AR, Chen L, et al. Site response in a layered liquefiable deposit: evaluation of different numerical tools and methodologies with centrifuge experimental results. *J Geotech Geoenviron Eng*. 2018;144(10):4018073.
27. Been K, Jefferies MG. A state parameter for sands. *Géotechnique*. 1985;35(2):99-112.
28. Wood DM, Belkheir K, Liu DF. Strain softening and state parameter for sand modeling. *Géotechnique*. 1994;42(2):335-339.
29. Taiebat M, Jeremić B, Dafalias YF, Kaynia AM, Cheng Z. Propagation of seismic waves through liquefied soils. *Soil Dyn Earthq Eng*. 2010;30(4):236-257.
30. Dafalias YF. Bounding surface plasticity. I: mathematical foundations and hypoplasticity. *J Eng Mech*. 1986;112(9):966-987.
31. Zhang JM. Cyclic critical stress state theory of sand with its application to geotechnical problems. *PhD Thesis*: Tokyo Institute of Technology, Tokyo, Japan; 1997.

How to cite this article: Barrero A, Taiebat M, Dafalias Y. Modeling cyclic shearing of sands in the semifluidized state. *Int J Numer Anal Methods Geomech*. 2020;44:371–388. https://doi.org/10.1002/nag.3007